interesting generalizations can be made. The Pt-centered clusters that have 16 valence electrons have flattened toroidal geometries, while those having 18 electrons have spheroidal geometries usually based on the icosahedron or the cube. This has been explained by the tensor surface harmonics theory introduced by Stone[11,33,34] and extended to include Au clusters by Mingos.[12] Recent work by Kanters et al.[3,6,7,35] and the results reported in this study show that this structural generalization works very well for Pt-centered L_yPtAu_x clusters. For example, the 18-electron clusters shown in Figure 3 all have spheroidal geometries that can be described as icosahedral fragments. In these structures the Pt-bound ligands (PPh_3 or CO) are positioned in the direction of other icosahedral vertices (vide supra). The 18-electron clusters $[(PPh_3)(H)Pt(AuPPh_3)_7]^{2+}$[4] and $[(C{\equiv}C{-}t\text{-}Bu)(PPh_3)Pt(AuPPh_3)_6]^{+}$[2] have distorted cubic geometries. The 16-electron Pt-centered clusters $[(PPh_3)Pt(AuPPh_3)_6]^{2+}$,[3] $[Pt(AuPPh_3)_8]^{2+}$,[6] and $[(AgNO_3)Pt(AuPPh_3)_8]^{2+}$[7] all have flattened toroidal geometries. Figures in ref 3, 6, and 7 clearly show the change from toroidal to spheroidal geometry for these three clusters, respectively, upon the addition of the 2-electron-donor ligand CO.

The utility of this simple electron counting formalism in predicting reactivity and structure in clusters of this type has been demonstrated in this and other studies and will guide future work in this area.

Acknowledgment. This work was supported by the National Science Foundation (Grant CHE-8818187) and by the University of Minnesota. We also thank the Fundação De Amparo A Pesquisa Do Estado De São Paulo for support of Dr. Felicissimo's visit to Minnesota. We are grateful for many helpful discussions with Prof. J. J. Steggerda and his co-workers.

Supplementary Material Available: Figures S1 and S2, displaying the PLUTO drawings of **8** and **11**, and Tables SI-SIX, listing complete crystal data and data collection parameters, general temperature factor expressions, final positional and thermal parameters for all atoms including solvate molecules, and distances and angles (30 pages); Tables SX and SXI, listing observed and calculated structure factor amplitudes (86 pages). Ordering information is given on any current masthead page.

(33) Stone, A. J. *Mol. Phys.* **1980**, *41*, 1339.
(34) Stone, A. J. *Polyhedron* **1984**, *3*, 1299.
(35) Kanters, R. P. F. Ph.D. Thesis, Nijmegen, The Netherlands, 1990, ISBN 90-9003290-8.

Contribution from the Department of Chemistry, University of Victoria, Victoria, British Columbia, Canada V8W 3P6

Synthesis and ^{31}P NMR Spectroscopy of Trinuclear, Phosphido-Bridged Iridium and Rhodium Clusters. Crystal and Molecular Structures of $[M_3(\mu\text{-}PPh_2)_3(CO)_nL_2]$ (M = Ir or Rh, n = 3, L_2 = Bis(diphenylphosphino)methane; M = Ir, n = 5, L = t-BuNC)

David E. Berry, Jane Browning, Khashayar Dehghan, Keith R. Dixon,* Neil J. Meanwell, and Andrew J. Phillips

Received June 14, 1990

Reaction of $[Ir_2(cyclooctene)_4Cl_2]$ with CO, $NHEt_2$, and $PHPh_2$ provides a synthetic route to the trinuclear, phosphido-bridged iridium clusters $[Ir_3(\mu\text{-}PPh_2)_3(CO)_nL_2]$ (n = 3, L = CO or PPh_3, L_2 = bis(diphenylphosphino)methane (dppm); n = 5, L = t-BuNC). The CO and PPh_3 complexes are analogues of previously known rhodium derivatives, and rhodium analogues of the dppm and t-BuNC complexes are also reported. $[Ir_3(\mu\text{-}PPh_2)_3(CO)_3(dppm)]$ (I) and $[Rh_3(\mu\text{-}PPh_2)_3(CO)_3(dppm)]$ (II) crystallize in the *Pnma* space group (Z = 4) with the following respective unit cell dimensions: a = 23.963 (5) Å, b = 24.970 (5) Å, c = 11.080 (2) Å; a = 24.031 (6) Å, b = 25.069 (9) Å, c = 11.117 (4) Å. $[Ir_3(\mu\text{-}PPh_2)_3(CO)_5(t\text{-}BuNC)_2]$ (III) crystallizes in the $P2_1/n$ space group (Z = 4) with a = 23.015 (4) Å, b = 20.197 (6) Å, c = 11.849 (5) Å, and β = 92.19 (4)°. The structures of I and II consist of approximately equailateral triangles of metal atoms (average M-M distances 2.78 (Ir) and 2.79 Å (Rh)), with the CO and two PPh_2 ligands lying approximately in the M_3 plane. The third PPh_2 bridge is approximately perpendicular to this plane, linking the two basal metal atoms, which are also bridged by the dppm ligand. In contrast, the structure of III has all three PPh_2 bridges approximately in the M_3 plane with the t-BuNC ligands added approximately perpendicular to this plane at the apical iridium. The Ir-Ir distances are much longer, averaging 3.23 Å. Complete analyses of ^{31}P NMR spectra are reported for I-III and for IV, the Rh analogue of III. The phosphido bridge shifts reflect the changes in metal-metal distances, with I and II strongly deshielded (by 80-240 ppm) relative to III and IV. There is also a general reduction in the one-bond Rh-P coupling constants in the 50-electron cluster, IV relative to the 46-electron cluster, II.

Introduction

A recurring theme of recent organometallic and cluster chemistry has been the study of metals linked by strong yet flexible bridges. Such bridges are able to preserve the integrity of a complex while permitting the making and breaking of metal-metal bonds. Two notable examples are the extensive studies of "A-frame" complexes in which two metals are linked by bis(diphenylphosphino)methane (dppm) bridges[1,2] and also the interest in phosphido (PR_2) bridges in both dinuclear and cluster complexes.[3-10] The trinuclear cluster $[Rh_3(\mu\text{-}PPh_2)_3(CO)_5]$[11,12] is an especially interesting example of the latter, involving one formal 16-electron metal center and two 18-electron centers. There are 46 cluster valence electrons, and the Rh-Rh bonds average 2.77 Å. In a carbon monoxide atmosphere, this complex can be converted to an unstable 50-electron derivative, $[Rh_3(\mu\text{-}PPh_2)_3(CO)_7]$, in which there are formally two 16-electron centers and one 18-electron center and in which the Rh-Rh distances average 3.15

(1) Puddephatt, R. J. *Chem. Soc. Rev.* **1983**, *12*, 99-127.
(2) Balch, A. L. In *Catalytic Aspects of Metal Phosphine Complexes*; Alyea, E. C., Meek, D. W., Eds.; Advances in Chemistry Series 196; American Chemical Society: Washington, DC, 1982; pp 243-255.
(3) Carty, A. J. In ref 2, pp 163-193.
(4) Yu, Y. F.; Chau, C. N.; Wojcicki, A.; Calligaris, M.; Nardin, G.; Balducci, G. *J. Am. Chem. Soc.* **1984**, *106*, 3704-3705.
(5) Regragui, R.; Dixneuf, P. H.; Taylor, N. J.; Carty, A. J. *Organometallics* **1984**, *3*, 1020-1025.
(6) Patel, V. D.; Taylor, N. J.; Carty, A. J. *J. Chem. Soc., Chem. Commun.* **1984**, 99-100.
(7) Regragui, R.; Dixneuf, P. H.; Taylor, N. J.; Carty, A. J. *Organometallics* **1984**, *3*, 814-816.
(8) Geoffroy, G. L.; Rosenberg, S.; Shulman, P. M.; Whittle, R. R. *J. Am. Chem. Soc.* **1984**, *106*, 1519-1521.
(9) Shyu, S. G.; Wojcicki, A. *Organometallics* **1984**, *3*, 809-812.
(10) Carty, A. J.; Maclaughlin, S. A.; Nucciarone, D. In *Phosphorus-31 NMR Spectroscopy in Stereochemical Analysis*; Verkade, J. G., Quin, L. D., Eds.; VCH Publishers Inc.: New York, 1987; pp 559-620.
(11) Haines, R. J.; Steen, N. D. C. T.; English, R. B. *J. Organomet. Chem.* **1981**, *209*, C34-36.
(12) Haines, R. J.; Steen, N. D. C. T.; English, R. B. *J. Chem. Soc., Dalton Trans.* **1984**, 515-525.

0020-1669/91/1330-0396$02.50/0

Å. This remarkable expansion from bonding to nonbonding distances is also present in $[Rh_3(\mu\text{-}PPh_2)_3(CO)_6(PPh_2H)]$ (3.17 Å)[12] but not in $[Rh_3(\mu\text{-}PPh_2)_3(CO)_3(PPh_3)_2]$ (2.78 Å).[13] Several aspects of this chemistry merit further attention. First, no ^{31}P NMR data are available, which is of considerable interest in view of the widespread use of phosphido bridge ^{31}P shifts for the diagnosis of metal–metal bonds.[10,14] Second, the ligand requirements for the change in bond distances are not known. Third, the chemistry of these clusters, for example oxidative-addition reactions at the two 16-electron centers of the 50-electron units, is potentially important and does not appear to have been further investigated. Finally, no iridium analogues have been studied with the exception of the synthesis of one sterically hindered example, $[Ir_3(\mu\text{-}P(t\text{-}Bu)_2)_3(CO)_5]$.[15]

We became interested in these complexes as an extension of our recent work on phosphido-bridged triangles containing Pt and Pd, and in particular their fragmentation reactions with dppm to new Pt(I) and Pd(I) derivatives.[14,16] In the present paper we describe a successful synthesis of the iridium analogue of $[Rh_3(\mu\text{-}PPh_2)_3(CO)_5]$ and its stabilization as the dppm derivative, $[Ir_3(\mu\text{-}PPh_2)_3(CO)_3(dppm)]$. The reaction with dppm results in substitution of CO, with essentially no change in the metal–metal bond lengths (2.78 Å), and contrasts strongly with the action of *tert*-butyl isocyanide under similar conditions. The latter ligand yields an addition product, $[Ir_3(\mu\text{-}PPh_2)_3(CO)_5(t\text{-}BuNC)_2]$, with essentially nonbonding metal–metal distances (3.23 Å). X-ray diffraction studies of $[Ir_3(\mu\text{-}PPh_2)_3(CO)_3(dppm)]$ (I), its rhodium analogue (II), and $[Ir_3(\mu\text{-}PPh_2)_3(CO)_5(t\text{-}BuNC)_2]$ (III) are reported, together with complete analyses of $^{31}P\{^1H\}$ NMR spectra for I–III and $[Rh_3(\mu\text{-}PPh_2)_3(CO)_5(t\text{-}BuNC)_2]$ (IV). Subsequent papers in this series will deal with other ligands, seeking to clarify the requirements for metal–metal bond elongation, and with oxidative addition chemistry.

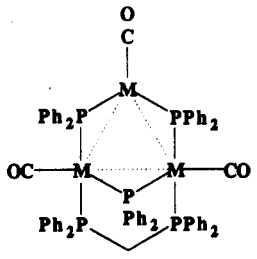

I (M = Ir)

II (M = Rh)

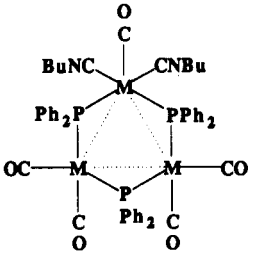

III (M = Ir)

IV (M = Rh)

Results

(a) Synthesis. Polynuclear, phosphido-bridged iridium clusters appear to be relatively rare, with only two previous examples: $[Ir_3(\mu\text{-}P(t\text{-}Bu)_2)_3(CO)_5]$[15] and $[Ir_4(\mu\text{-}PCy_2)_4(CO)_6]$.[17] The main obstacles to synthesizing such compounds seem to arise from a lack of suitable starting materials and an apparent preference for formation of dinuclear species. For example, $[Rh_2Cl_2(CO)_4]$ is a valuable cluster precursor, while $[Ir_2Cl_2(CO)_4]$ is a highly insoluble polymeric material. Also, while $[RhH(CO)(PPh_3)_3]$ thermally decomposes to $[Rh_3(\mu\text{-}PPh_2)_3(CO)_3(PPh_3)_2]$, $[IrH(CO)(PPh_3)_3]$ under similar conditions produces $[Ir_2(\mu\text{-}PPh_2)_2(CO)_6]$.[13,18,19] We find that treatment of the iridium dimer $[Ir_2(cyclooctene)_4Cl_2]$ with carbon monoxide, followed by reaction with base and then diphenylphosphine, produces a mixture of two products. Complete characterization of these products has not been possible at this stage, but there is strong evidence to suggest that they are the related trinuclear clusters $[Ir_3(\mu\text{-}PPh_2)_3(CO)_5]$ and $[Ir_3(\mu\text{-}PPh_2)_3(CO)_6]$. The $^{31}P\{^1H\}$ NMR spectrum of a dichloromethane solution of the mixture is in good agreement with this assignment. The spectrum consists of three signals: triplet, doublet, and singlet at −40.5, 99.5, and 38.8 ppm, respectively. The triplet and doublet are mutually coupled ($^2J(P\text{–}P) = 15$ Hz) and can be attributed to the unsymmetrical pentacarbonyl, while the singlet is assignable to the fully symmetrical hexacarbonyl. Saturation of this solution with carbon monoxide causes the spectrum to collapse to the singlet signal. Subsequent removal of solvent in vacuo regenerates the triplet and doublet signals, showing that there is a labile equilibrium between the penta- and hexacarbonyl species.

The mixture of carbonyl compounds reacts readily and rapidly with a variety of mono- and bidentate ligands to give substituted derivatives of the parent clusters. Thus reaction with triphenylphosphine readily displaces two carbonyl ligands to yield $[Ir_3(\mu\text{-}PPh_2)_3(CO)_3(PPh_3)_2]$, the analogue of the rhodium cluster $[Rh_3(\mu\text{-}PPh_2)_3(CO)_3(PPh_3)_2]$, made previously from $[RhH(CO)(PPh_3)_3]$.[13] Similarly, dppm displaces CO to yield I. However, *tert*-butyl isocyanide reacts by addition of the isocyanide to the unique iridium position to yield III, rather than a substitution product. III can also be prepared in better yield by reaction of *tert*-butyl isocyanide with $[Ir_3(\mu\text{-}PPh_2)_3(CO)_3(PPh_3)_2]$. The rhodium analogues, II and IV, are also synthesized by reactions of $[Rh_3(\mu\text{-}PPh_2)_3(CO)_3(PPh_3)_2]$ with the appropriate ligands.

(b) $^{31}P\{^1H\}$ Nuclear Magnetic Resonance Spectra. The parameters for these spectra are collected in Table I. The atom-labeling scheme used in Table I and the following discussion is shown in structure V.

Table I. ^{31}P NMR[a] Chemical Shifts (ppm) and Coupling Constants (Hz) for $[Ir_3(\mu\text{-}PPh_2)_3(CO)_3(dppm)]$ (I), $[Rh_3(\mu\text{-}PPh_2)_3(CO)_3(dppm)]$ (II), $[Ir_3(\mu\text{-}PPh_2)_3(CO)_5(t\text{-}BuNC)_2]$ (III), and $[Rh_3(\mu\text{-}PPh_2)_3(CO)_5(t\text{-}BuNC)_2]$ (IV)

	I	II	III	IV
$\delta(1,1')$	+100.7	+152.1	−139.4	−43.8
$\delta(2)$	−21.7	+74.0	−104.6	−11.3
$\delta(3,3')$	−155.9	−127.1		
$J(1,1')$	*b*	160	*b*	160
$J(1,2)$	24	25	144	160
$J(1,4)$		128		35
$J(1,5)$		104		70–90
$J(1,5')$		0		70–50
$J(2,3)$	169	151		
$J(2,5)$		128		88
$J(3,3')$	*b*	54		
$J(3,5)$		132		

[a] The atom-labeling scheme is that shown in structure V. All coupling constants that are not listed were less than the spectrum resolution of about 5 Hz. [b] Not available from observed spectrum.

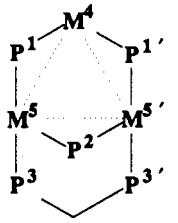

V: generalized atom labels for Table I and NMR discussion

$[Ir_3(\mu\text{-}PPh_2)_3(CO)_3(dppm)]$ (I). This complex exhibits a straightforward first-order spectrum in which a doublet at −155.9 ppm is easily assigned to the phosphorus of the dppm ligand. The large doublet coupling ($J(2,3) = 169$ Hz) is due to the unique

(13) Billig, E.; Jamerson, J. D.; Pruett, R. L. *J. Organomet. Chem.* **1980**, *192*, C49–51.

(14) Berry, D. E.; Bushnell, G. W.; Dixon, K. R.; Moroney, P. M.; Wan, C. *Inorg. Chem.* **1985**, *24*, 2625–2634.

(15) Arif, A. M.; Heaton, D. E.; Jones, R. A.; Kidd, K. B.; Wright, T. B.; Whittlesey, B. R.; Atwood, J. L.; Hunter, W. E.; Zhang, H. *Inorg. Chem.* **1987**, *26*, 4065–4073.

(16) Hadj-Bagheri, N.; Browning, J.; Dehghan, K.; Dixon, K. R.; Meanwell, N. J.; Vefghi, R. *J. Organomet. Chem.* **1990**, *396*, C47–C52.

(17) Arif, A. M.; Jones, R. A.; Schwab, S. T.; Whittlesey, B. R. *J. Am. Chem. Soc.* **1986**, *108*, 1703–1705.

(18) Mason, R.; Søtofte, S. T.; Robinson, S. D.; Uttley, M. F. *J. Organomet. Chem.* **1972**, *46*, C61–62.

(19) Bellon, P. L.; Benedicenti, C.; Caglio, G.; Manassero, M. *J. Chem. Soc., Chem. Commun.* **1973**, 946–947.

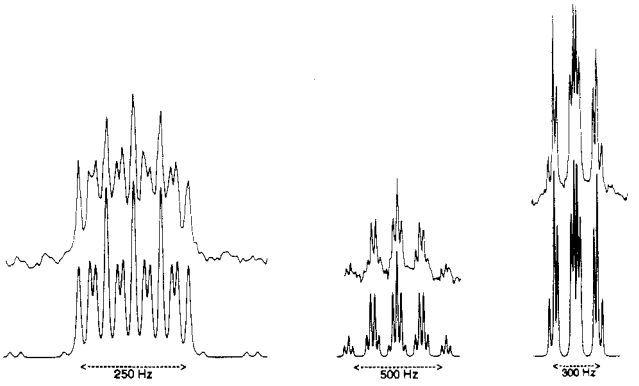

Figure 1. Observed (upper trace) and simulated (lower trace) $^{31}P\{^1H\}$ NMR spectra of $[Rh_3(\mu\text{-}PPh_2)_3(CO)_3(\mu\text{-dppm})]$ (II) at 101.3 MHz. From left to right, the three resonances are centered at +152.1, +74.0, and −127.1 ppm, respectively, relative to H_3PO_4.

phosphorus bridge, P(2), which is in a pseudotrans relationship with P(3) and P(3′), P–Ir–P = 140°. A second doublet at +100.7 ppm is assigned to the bridging phosphides, P(1,1′), $J(1,2)$ = 24 Hz, and is highly deshielded by the Ir–Ir bond. Finally, P(2) appears as the expected triplet of triplets due to $J(1,2)$ and $J(2,3)$. Interestingly, this phosphido bridge is much more shielded, −21.7 ppm, then the P(1,1′) resonance, presumably due to the fact that the plane of the P(2) bridge is almost perpendicular to the Ir_3 plane. It is also noteworthy that $J(1,3)$, the coupling between the dppm phosphorus and the P(1,1′) bridges, is less than the spectrum resolution of about 5 Hz.

$[Rh_3(\mu\text{-}PPh_2)_3(CO)_3(dppm)]$ (II). This spectrum is much more complex owing to the presence of ^{103}Rh ($I = {}^1/_2$, 100%), and the spectrum is shown in Figure 1 together with a computer simulation based on the parameters from Table I.

By analogy with the spectrum of the iridium compound above, multiplets at +152.1, +74.0, and −127.1 ppm are assigned to P(1,1′), P(2), and P(3,3′), respectively. Initial examination of the P(3,3′) resonance suggests that it may be interpreted as the AA′ region of an AA′XX′ spin system,[20,21] which has been doubled by a subsequent first-order coupling of about 151 Hz. This analysis seems reasonable since, on the basis of the Ir analogue, $J(1,3)$ is expected to be small. Also, $J(3,4)$, a P–Rh coupling transmitted through two almost perpendicular bonds (P–Rh–Rh = 100.6°), is expected to be small; and the shift coupling ratio indicates that $J(2,3)$ should be first order. Under these conditions, P(3,3′) and Rh(5,5′) may be treated as an AA′XX′ system doubled by further coupling to P(2). Normally, the AA′ region of an AA′XX′ system consists of a strong doublet, separated by $J(A,X) + J(A,X')$, together with two quartets defined by the following secondary parameters: L, $J(A,X) - J(A,X')$; K, $J(A,A') + J(X,X')$; M, $J(A,A') - J(X,X')$. However, several deceptively simple cases of this spin system are relatively common. The first arises when M = K and the quartets are coincident. When this condition is met and also $L \ll K$, one of two other deceptively simple spectra may arise. If the center peaks of the quartets are still resolved but the outer lines are too weak to observe, then a 1:1:1:1 four-line pattern results.[21] More extreme cases produce additional merging of the two central lines, giving an apparent 1:2:1 triplet. In the present case, removal of $J(2,3)$ from the observed P(3,3′) resonance leaves a fairly typical pattern of the first type, clearly showing the major doublet, but the two quartets are coincident within spectrum resolution.

With these assumptions, analysis of the P(3,3′) resonance was completed according to the standard AA′XX′ equations. The coincidence of the quartets shows that the sum of $J(A,A')$ and $J(X,X')$ is approximately equal to their difference, and thus either

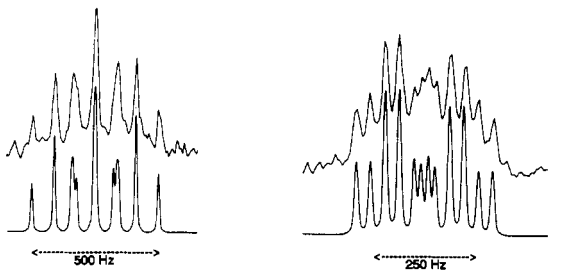

Figure 2. Observed (upper trace) and simulated (lower trace) $^{31}P\{^1H\}$ NMR spectra of $[Rh_3(\mu\text{-}PPh_2)_3(CO)_5(t\text{-}BuNC)_2]$ (IV) at 101.3 MHz. The left- and right-hand resonances are centered at −11.3 and −43.8 ppm, respectively, relative to H_3PO_4.

$J(3,3')$ or $J(5,5')$ is much larger than the other. Since Pt–Pt couplings in related triangular systems are normally relatively small, for example in $[Pt_3(t\text{-}BuNC)_6]$, 188 Hz, or $[Pt_3(CO)_3(PBu_2Me)_3]$, 1770 Hz,[22] and the magnetogyric ratio for Rh is only −0.85 compared with 5.84 for Pt, it is probable that $J(5,5')$ is small (<5 Hz) rather than $J(3,3')$.[23] Moreover, $J(3,3')$ is a two-bond P–P coupling via carbon and is expected to be relatively large. For example, in noncoordinated dppm $^2J(P\text{–}P)$ is +125 Hz.[24] This value is frequently reduced by negative contributions through the metal when dppm is coordinated,[25,26] but the proposed value of 54 Hz (Table I) is well within the normal range.

Moving to the lowest field resonance in Figure 1, we can assign this as P(1,1′) and apply a similar analysis. Removal of first-order couplings to P(2), 25 Hz, and Rh(4), 128 Hz, leaves a four-line pattern for the AA′ region of the AA′XX′ system composed of P(1,1′) and Rh(5,5′). This four-line pattern is an example of the second deceptively simple case mentioned above, which occurs when the quartets are superimposed, $J(A,A') \gg J(X,X')$ or $J(X,X') \gg J(A,A')$, and the outer lines are very weak, $(J(A,X) - J(A,X')) \ll (J(A,A') + J(X,X'))$.[21] Both of these conditions are met in the present case since $J(5,5')$, i.e. $J(X,X')$, is small and $J(1,1')$, an approximately trans P–Rh–P coupling (159°), is likely large compared with the difference of $J(1,5)$ and $J(1,5')$, i.e. $J(AA') \gg J(A,X) - J(A,X')$.

With preliminary parameters from the preceding analysis in hand, the P(2) resonance can be understood as approximately an overlapping triplet of triplet of triplets due to coupling to P(1,1′), P(3,3′), and Rh(5,5′), and final refinement and simulation of the complete spectrum gives Figure 1 and the parameters shown in Table I. The value of $J(1,1')$ can only be an estimate with wide latitude, e.g. 100–200 Hz. The values of $J(1,5)$ and $J(1,5')$ are shown in Table I as 104 and 0 Hz, but values of $J(1,5')$ up to about 10 Hz will not affect the analysis, provided of course that $J(1,5)$ is adjusted to maintain the sum constant at 104 Hz. Larger values of $J(1,5')$ are not acceptable.

$[Ir_3(\mu\text{-}PPh_2)_3(CO)_5(t\text{-}BuNC)_2]$ (III). This spectrum is simple first order, showing a doublet (−139.4 ppm) and triplet (−104.6 ppm), due to P(1,1′) and P(2), respectively. The noteworthy features relative to the spectrum of $[Ir_3(\mu\text{-}PPh_2)_3(CO)_3(dppm)]$ are the dramatic increase in shielding of the bridging phosphorus atoms, correlating with the large increase in Ir–Ir distance from about 2.8 to 3.2 Å, and the increase in $J(1,2)$ from 24 Hz for $[Ir_3(\mu\text{-}PPh_2)_3(CO)_3(dppm)]$, where P(2) lies approximately perpendicular to the Ir_3 plane, to 144 Hz for the present complex, where P(2) is approximately in the Ir_3 plane. The corresponding P–M–P angles are 108 and 150°, respectively.

$[Rh_3(\mu\text{-}PPh_2)_3(CO)_5(t\text{-}BuNC)_2]$ (IV). As was the case for the dppm complexes, the spectrum for the rhodium cluster is much

(20) Pople, J. A.; Schneider, W. G.; Bernstein, H. J. *High Resolution Nuclear Magnetic Resonance*; McGraw-Hill: New York, 1959; pp 138–142.
(21) Cartwright, S. J.; Dixon, K. R.; Rattray, A. D. *Inorg. Chem.* **1980**, *19*, 1120–1124.
(22) Boag, N. M.; Browning, J.; Crocker, C.; Goggin, P. L.; Goodfellow, R. J.; Murray, M.; Spencer, J. L. *J. Chem. Res., Synop.* **1978**, 228–229.
(23) Mann, B. E.; Meanwell, N. J.; Spencer, C. M.; Taylor, B. F.; Maitlis, P. M. *J. Chem. Soc., Dalton Trans.* **1985**, 1555–1559.
(24) Colquhoun, I. J.; McFarlane, W. *J. Chem. Soc., Dalton Trans.* **1982**, 1915–1921.
(25) Crumbliss, A. L.; Topping, R. J. In ref 10, pp 531–558.
(26) Berry, D. E.; Browning, J.; Dixon, K. R.; Hilts, R. W. *Can. J. Chem.* **1988**, *66*, 1272–1282.

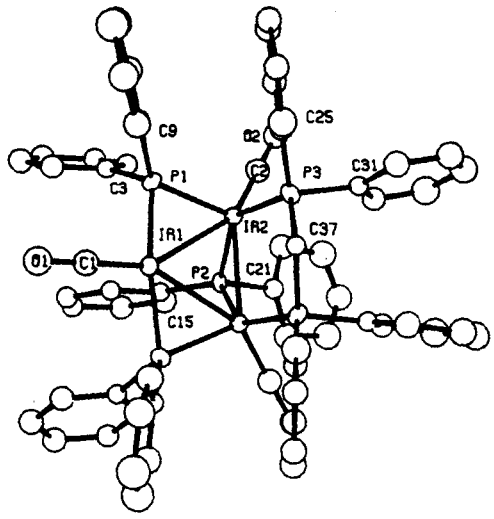

Figure 3. ORTEP plot of $[Ir_3(\mu\text{-}PPh_2)_3(CO)_3(\mu\text{-dppm})]$ (I). There is a crystallographic plane of symmetry through O(1), C(1), Ir(1), P(2), C(15), and C(21).

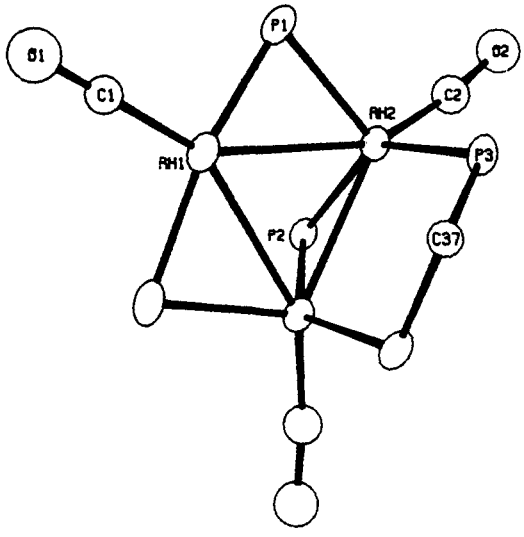

Figure 4. ORTEP plot of the metal triangle and ligating atoms of $[Rh_3(\mu\text{-}PPh_2)_3(CO)_3(\mu\text{-dppm})]$ (II). All phenyl groups have been omitted. There is a crystallographic plane of symmetry through O(1), C(1), Rh(1), P(2), and C(37).

more complex. The observed spectrum is shown together with a computer simulation in Figure 2.

The P(2) resonance at −11.3 ppm is a comparatively straightforward, overlapping triplet of triplets due to $J(1,2)$, 160 Hz, and $J(2,4)$, 88 Hz. However, the P(1,1′) resonance at −43.8 ppm is more complex, appearing roughly as a doublet (160 Hz) of triplet (71 Hz) of doublets (35 Hz). Assuming first-order coupling for $J(1,2)$ of 160 Hz and for $J(1,4)$ of 35 Hz, this leaves only an apparent triplet as the A portion of the AA′XX′ system composed of P(1,1′) and Rh(5,5′). Such triplets represent the extreme deceptively simple case mentioned above. In the present system, $J(1,1')$ and $J(5,5')$ are likely similar to the values for $[Rh_3(\mu\text{-}PPh_2)_3(CO)_3(dppm)]$, i.e. 160 and <5 Hz. Thus, $J(A,A') \gg J(X,X')$ and the quartets will be coincident. If triplets are to be observed, it is also necessary that $J(1,5) - J(1,5')$ be much smaller than $J(1,1')$, and the triplet spacing requires that $J(1,5)$ and $J(1,5')$ average to 71 Hz. With these requirements, simulations show that $J(1,5)$ and $J(1,5')$ could be as different as 91 and 51 Hz but not more different. Thus, there has been a major increase in $J(1,5')$ relative to the <10 Hz observed for the dppm complex, II.

(c) X-ray Structures. The structures of compounds I ($[Ir_3(\mu\text{-}PPh_2)_3(CO)_3(dppm)]$), II ($[Rh_3(\mu\text{-}PPh_2)_3(CO)_3(dppm)]$), and III ($[Ir_3(\mu\text{-}PPh_2)_3(CO)_5(t\text{-}BuNC)_2]$) are shown as ORTEP diagrams

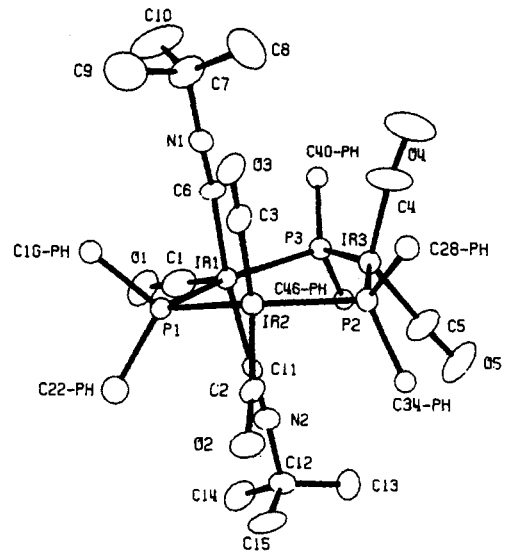

Figure 5. ORTEP plot of $[Ir_3(\mu\text{-}PPh_2)_3(CO)_5(t\text{-}BuNC)_2]$ (III). Only the first atom of each phenyl ring is shown.

Table II. Selected Crystallographic Data for $[Ir_3(\mu\text{-}PPh_2)_3(CO)_3(dppm)]$ (I), $[Rh_3(\mu\text{-}PPh_2)_3(CO)_3(dppm)]$ (II), and $[Ir_3(\mu\text{-}PPh_2)_3(CO)_5(t\text{-}BuNC)_2]$ (III)

	I	II	III
formula	$C_{64}H_{52}O_3P_5Ir_3$	$C_{64}H_{52}O_3P_5Rh_3$	$C_{51}H_{48}N_2O_5P_3Ir_3$
fw	1600.7	1332.7	1438.5
space group	*Pnma* (No. 62)	*Pnma* (No. 62)	$P2_1/n$ (No. 14)
a, Å	23.963 (5)	24.031 (6)	23.015 (4)
b, Å	24.970 (5)	25.069 (9)	20.197 (6)
c, Å	11.080 (2)	11.117 (4)	11.849 (5)
β, deg	90.00	90.00	92.19 (4)
V, Å^3	6630	6697	5504
Z	4	4	4
density, g cm^{-3}: calc/obs	1.60/1.63	1.32/1.43	1.74/1.77
diffractometer	Enraf-Nonius CAD4	Picker four-circle	Enraf-Nonius CAD4
radiation (λ, Å)	Mo Kα (0.71069)	Mo Kα (0.71069)	Mo Kα (0.71069)
μ, cm^{-1}	65.34	8.69	73.40
transm factor range		0.69–0.78	
temp, K	295	295	295
no. of indep reflcns	2804	6045	4570
R^a	0.069	0.10	0.059
$R_w{}^a$	0.064	0.10	0.056

$^a \sum w\Delta^2$; $w = 1/(\sigma^2(F) + 0.001F^2)$; $\Delta = ||F_o| - |F_c||$. $R = (\sum\Delta/\sum F_o)$; $R_w = (\sum w\Delta^2/\sum wF_o^2)^{1/2}$.

in Figures 3–5, respectively. Unit cell and other parameters related to the crystal structure determination are given in Table II. Selected bond lengths and angles are shown in Table III together with comparison data for VI ($[Rh_3(\mu\text{-}PPh_2)_3(CO)_5]$) and VII ($[Rh_3(\mu\text{-}PPh_2)_3(CO)_7]$).[12] In order to simplify comparisons, Table III and the following discussion use the standardized labeling scheme shown in structure VIII and discussed in footnote *a* of Table III.

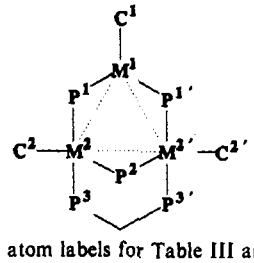

VIII: generalized atom labels for Table III and X-ray discussion

The structures of I and II are essentially similar to that of VI. In each case, there is an almost planar M_3P_2 core and the third phosphido bridge is bent so its M–P–M plane is almost perpendicular to the core. Thus, P(1) and P(1′) are only slightly out

Table III. Selected[a] Interatomic Distances (Å) and Angles (deg) for $[Ir_3(\mu\text{-}PPh_2)_3(CO)_3(dppm)]$ (I), $[Rh_3(\mu\text{-}PPh_2)_3(CO)_3(dppm)]$ (II), $[Ir_3(\mu\text{-}PPh_2)_3(CO)_5(t\text{-}BuNC)_2]$ (III), $[Rh_3(\mu\text{-}PPh_2)_3(CO)_5]$ (VI),[b] and $[Rh_3(\mu\text{-}PPh_2)_3(CO)_7]$ (VII)[b]

	I	II	III	VI	VII
M(1)-M(2)	2.805 (2)	2.796 (3)	3.176 (2), 3.199 (2)	2.800 (1)	3.10 (1)
M(2)-M(2′)	2.744 (3)	2.765 (4)	3.329 (2)	2.698 (1)	3.22 (1)
P(1)-M(1)	2.270 (8)	2.269 (8)	2.373 (7), 2.378 (7)	2.266 (2)	2.37 (3)
P(1)-M(2)	2.289 (8)	2.288 (6)	2.273 (7), 2.300 (8)	2.292 (2)	2.27 (3)
P(2)-M(2)	2.292 (10)	2.290 (7)	2.321 (7), 2.332 (7)	2.288 (2)	2.38 (4)
P(3)-M(2)	2.327 (9)	2.345 (6)			
C(1)-M(1)	1.74 (6)	1.76 (4)	1.80 (4)	1.804 (8)	1.85 (2)
C(2)-M(2)	1.77 (4)	1.82 (3)		1.872 (9)	
M(2)-M(1)-M(2′)	58.6 (1)	59.3 (1)	63.0 (1)	57.6 (1)	62.5 (3)
P(1)-M(1)-P(1′)	157.7 (3)	159.5 (3)	154.3 (3)	162.1 (1)	156 (1)
C(1)-M(1)-P(1)	99.0 (3)	98.4 (2)	102.4 (11), 103.3 (11)	98.9 (3)	102 (2)
C(1)-M(1)-M(2)	150.6 (2)	150.3 (1)	147.7 (11), 148.6 (11)	150.6 (3)	149 (2)
M(1)-M(2)-M(2′)	60.7 (1)	60.4 (1)	58.8 (1), 58.2 (1)	61.2 (1)	58.7 (3)
P(1)-M(2)-P(2)	107.6 (4)	107.7 (3)	150.1 (3), 149.4 (3)	108.6 (1)	154 (1)
P(1)-M(2)-P(3)	104.3 (3)	104.9 (2)			
P(2)-M(2)-P(3)	140.5 (3)	139.4 (3)			
C(2)-M(2)-P(1)	103 (1)	101 (1)		105.0 (3)	
C(2)-M(2)-P(2)	99 (1)	101 (1)		97.7 (2)	
C(2)-M(2)-P(3)	96 (1)	96 (1)			
C(2)-M(2)-M(1)	152 (1)	151 (1)	150.7 (2)		
C(2)-M(2)-M(2′)	141 (1)	143 (1)		138.3 (3)	
M(1)-P(1)-M(2)	75.9 (2)	75.7 (2)	86.2 (2), 86.3 (2)	75.8 (1)	84 (1)
M(2)-P(2)-M(2′)	73.5 (4)	74.3 (3)	91.4 (3)	72.3 (1)	85 (1)

[a] The atom-labeling scheme is that shown in structure VIII and is adopted only for convenience of comparison. Note that only I and II actually possess the crystallographic planes of symmetry implied by the primed labels. Thus, for III, the atoms labeled M(2′) and P(1′) in this table and structure VIII are actually M(3) and P(3) in the ORTEP diagrams and other tables. For VI and VII, the numbering schemes used by the original authors were quite different. For III, the two similar but crystallographically distinct parameters are shown (e.g. M(1)-M(2) and M(1)-M(3) are listed under M(1)-M(2)), but for VI and VII, only averages are shown for comparison purposes. Data are included in the table only where a direct comparison is meaningful. For example: at M(2), the orientations of the P(3)-M-C(2) or C(1)-M-C(2) fragments of I, II, and VI are quite different from the orientations of the $M(CO)_2$ fragments of III and VII, and no comparison is included. [b] Data from ref 12.

Table IV. Selected Fractional Atomic Coordinates and Temperature Parameters for $[Ir_3(\mu\text{-}PPh_2)_3(CO)_3(dppm)]$[a] (I)

atom	x/a	y/b	z/c	U_{eq}, Å^2
Ir(1)	47229 (9)	75000 (0)	-1284 (18)	431 (7)
Ir(2)	56947 (6)	69506 (5)	5481 (12)	377 (5)
P(1)	4823 (4)	6608 (3)	204 (8)	44 (3)
P(2)	5637 (5)	7500 (0)	2200 (11)	39 (5)
P(3)	6138 (4)	6895 (4)	-1316 (8)	44 (3)
O(1)	353 (2)	750 (0)	-105 (4)	93 (13)′
O(2)	630 (1)	600 (1)	156 (2)	76 (8)′
C(1)	404 (2)	750 (0)	-69 (5)	75 (18)′
C(2)	605 (2)	640 (2)	121 (3)	70 (12)′
C(3)	445 (1)	633 (1)	152 (2)	49 (10)′
C(9)	464 (1)	611 (1)	-92 (2)	47 (9)′
C(15)	507 (2)	750 (0)	329 (4)	46 (14)′
C(21)	631 (2)	750 (0)	314 (4)	53 (15)′
C(25)	594 (1)	636 (1)	-235 (2)	60 (11)′
C(31)	689 (1)	684 (1)	-118 (2)	49 (10)′
C(37)	607 (2)	750 (0)	-228 (4)	42 (13)′

[a] Estimated standard deviations are given in parentheses. Coordinates $\times 10^n$ where $n = 5$ for Ir, 4 for P, and 3 otherwise. Temperature parameters $\times 10^n$ where $n = 4$ for Ir and 3 otherwise. U_{eq} (the equivalent isotropic temperature parameter) $= {}^1/_3\sum_i\sum_j U_{ij}a_i^*a_j^*(a_i\cdot a_j)$. Primed values indicate that U_{iso} is given. $T = \exp[-(8\pi^2U_{iso}(\sin^2\theta)/\lambda^2)]$.

Table V. Selected Fractional Atomic Coordinates and Temperature Parameters for $[Rh_3(\mu\text{-}PPh_2)_3(CO)_3(\mu\text{-}dppm)]$[a] (II)

atom	x/a	y/b	z/c	U_{eq}, Å^2
Rh(1)	47460 (11)	75000 (0)	-743 (25)	494 (10)
Rh(2)	57151 (7)	69486 (9)	5526 (16)	423 (6)
P(1)	4845 (2)	6609 (3)	220 (5)	50 (2)
P(2)	5665 (4)	7500 (0)	2191 (8)	40 (3)
P(3)	6163 (2)	6903 (3)	-1320 (5)	47 (2)
O(1)	359 (1)	750 (0)	-93 (3)	111 (12)′
O(2)	628 (1)	599 (1)	157 (2)	88 (7)′
C(1)	405 (2)	750 (0)	-58 (3)	59 (10)′
C(2)	606 (1)	637 (1)	121 (3)	64 (8)′
C(3)	447 (1)	634 (1)	151 (1)	56 (7)′
C(9)	467 (1)	613 (1)	-87 (1)	60 (8)′
C(15)	510 (1)	750 (0)	332 (3)	34 (8)′
C(21)	630 (2)	750 (0)	322 (3)	54 (10)′
C(25)	599 (1)	637 (1)	-234 (1)	48 (7)′
C(31)	693 (1)	682 (1)	-123 (2)	59 (7)′
C(37)	608 (1)	750 (0)	-225 (3)	52 (10)′

[a] Estimated standard deviations are given in parentheses. Coordinates $\times 10^n$ where $n = 5$ for Rh, 4 for P, and 3 otherwise. Temperature parameters $\times 10^n$ where $n = 4$ for Rh and 3 otherwise. U_{eq} (the equivalent isotropic temperature parameter) $= {}^1/_3\sum_i\sum_j U_{ij}a_i^*a_j^*(a_i\cdot a_j)$. Primed values indicate that U_{iso} is given. $T = \exp[-(8\pi^2U_{iso}(\sin^2\theta)/\lambda^2)]$.

of the M_3 plane, at ±0.28, ±0.25, and ±0.29 Å in I, II, and VI, respectively. In I and II, the dihedral angles between the P(1)-M(1)-M(2) and M_3 planes are 8.9 and 7.8°, whereas the corresponding angles involving P(2)-M(2)-M(2′) and M_3 are 103.5 and 102.9°. Also in I and II, there is a molecular symmetry plane through O(1)-C(1)-M(1)-P(2) and the midpoint of M(2)-M(2′). The dppm ligands of I and II simply replace the axial CO ligands of VI with little change in the geometry at M(2). All the angles of I and II involving P(3) at M(2) are similar to corresponding angles involving the axial CO of VI. The dppm ligands are almost perpendicular to the M_3 planes with the M(2)-M(2′)-P(3)-P(3′) planes at 80.6 and 79.3° to the M_3 planes in I and II, respectively. This places the phosphorus atoms of dppm in a pseudotrans relationship with the bridging phosphide, P(2), with P(2)-M(2)-P(3) angles of 140.5 (3) and 139.4 (3)°. This relation is also seen in the angles, 22.9 and 23.5°, between the M(2)-M(2′)-P(3)-P(3′) and P(2)-M(2)-M(2′) planes.

Metal–metal distances are closely similar in I and II, at 2.744 (3) and 2.805 (2) Å for Ir and 2.765 (4) and 2.796 (3) Å for Rh. In each case, the unique edge is slightly shorter, and the metal triangle in VI is similar, with distances of 2.698 (1), 2.793 (1), and 2.806 (1) Å.

In comparison to the case of compounds I, II, and VI, the additional *t*-BuNC ligands coordinated at M(1) in III are added approximately perpendicular to the M_3 plane, C(6)-M(1)-C(11) is 170 (1)°, and the C–M–M angles average 86 ± 3°. Otherwise, the geometry at M(1) involving the equatorial CO, the phosphorus bridges, and the M–M–M angle is surprisingly little affected (see Table III). The axial CO ligands at M(1) in compound VII occupy positions very similar to those of the isocyanides of III,

Table VI. Selected Fractional Atomic Coordinates and Temperature Parameters for $[Ir_3(\mu\text{-}PPh_2)_3(CO)_5(t\text{-}BuNC)_2]$[a] (III)

atom	x/a	y/b	z/c	U_{eq}, Å^2
Ir(1)	62805 (5)	18497 (5)	-42479 (9)	397 (4)
Ir(2)	76040 (5)	19694 (6)	-34115 (9)	419 (4)
Ir(3)	72027 (5)	21918 (6)	-61143 (10)	445 (5)
P(1)	6785 (3)	1737 (3)	-2474 (6)	41 (3)
P(2)	8082 (3)	2071 (4)	-5092 (6)	44 (3)
P(3)	6206 (3)	2093 (4)	-6211 (6)	46 (3)
O(1)	508 (1)	146 (1)	-371 (2)	10 (1)
O(2)	832 (1)	80 (1)	-265 (2)	9 (1)
O(3)	783 (1)	339 (1)	-266 (2)	13 (1)
O(4)	738 (1)	364 (1)	-661 (3)	13 (2)
O(5)	743 (1)	109 (2)	-778 (2)	12 (1)
N(1)	619 (1)	333 (1)	-372 (2)	6 (1)
N(2)	658 (1)	39 (1)	-487 (2)	6 (1)
C(1)	555 (2)	162 (2)	-392 (3)	7 (2)
C(2)	799 (1)	124 (2)	-303 (3)	6 (1)
C(3)	771 (2)	285 (2)	-295 (3)	8 (2)
C(4)	732 (2)	309 (2)	-638 (3)	9 (2)
C(5)	733 (2)	148 (2)	-715 (3)	8 (2)
C(6)	624 (1)	278 (2)	-394 (3)	6 (1)
C(7)	618 (2)	409 (1)	-337 (4)	8 (2)
C(11)	646 (1)	93 (2)	-464 (2)	5 (1)
C(12)	665 (1)	-33 (1)	-516 (3)	7 (2)
C(16)	653 (1)	228 (1)	-138 (2)	4 (1)′
C(22)	673 (1)	93 (1)	-175 (2)	6 (1)′
C(28)	862 (1)	273 (1)	-521 (2)	4 (1)′
C(34)	852 (1)	135 (1)	-543 (2)	3 (1)′
C(40)	574 (1)	278 (1)	-656 (2)	5 (1)′
C(46)	590 (1)	141 (1)	-710 (2)	4 (1)′

[a] Estimated standard deviations are given in parentheses. Coordinates $\times 10^n$ where $n = 5$ for Ir, 4 for P, and 3 otherwise. Temperature parameters $\times 10^n$ where $n = 4$ for Ir, 3 for P, and 2 otherwise. U_{eq} (the equivalent isotropic temperature parameter) $= {}^1/_3\sum_i\sum_j U_{ij}a_i^*a_j^*(a_i\cdot a_j)$. Primed values indicate that U_{iso} is given. $T = \exp[-(8\pi^2U_{iso}(\sin^2\theta)/\lambda^2)]$.

with the corresponding C–M–C and C–M–M angles 152 and 79 ± 5°.[12] The most dramatic change occasioned by the additional ligands is the increase in the average M–M bond lengths from 2.77 Å in I, II, and VI to 3.19 Å in III and VII. These values may be compared with previous Ir–Ir single- and double-bond lengths of about 2.55 and 2.7–2.8 Å, respectively.[17,19] The increased M–M distances in III and VII are accompanied by movement of the unique phosphorus bridge, P(2), from almost perpendicular to the M_3 plane to an approximately in-plane position. Thus, the dihedral angle between the M_3 and P(2)–M(2)–M(2′) planes in I is 103.5° compared with 10.6° for the corresponding dihedral angle in III. The increase in the M(1)–M(2) bond length is accommodated by the phosphorus bridges in two ways: P(1)–M(1) increases from 2.27 to 2.37 Å, and the M–P–M angle opens from 76 to 86°. The P(1)–M(2) distance is not significantly affected. Similarly, at P(2) the P–M lengths increase from 2.29 to 2.33 Å and the M–P–M angle increases from 74 to 91°.

Discussion

The most important general question raised by these results concerns the ligand requirements for the two different types of observed reactivity. The 46-electron complexes, $[M_3(\mu\text{-}PPh_2)_3(CO)_5]$, react with extra ligands to yield either net substitution, as with dppm, or addition products, as with *t*-BuNC. Mechanistically, the substitution products may arise by simple substitution, but we have no evidence to exclude the alternative, and possibly more likely, mechanism of initial addition at the formally open coordination site of the apical metal atom. This could be followed by substitution of the free end of dppm for CO at a second metal atom and, finally, elimination of CO at the third metal atom. In any event, the net reaction is substitution at the basal metal atoms and there is essentially no change of geometry. In particular, the short M–M bond distances are retained. The addition reactions occur at the apical metal, the cluster valence electron count rises to 50, the M_3P_3 unit becomes approximately planar, and the M–M lengths increase to essentially nonbonding distances. Known examples to date: substitution products, $[M_3(\mu\text{-}PPh_2)_3(CO)_3L_2]$ (L = PPh_3,[13] L_2 = dppm); addition products, $[M_3(\mu\text{-}PPh_2)_3(CO)_5L_2]$ (L = CO[12] or *t*-BuNC, L_2 = (CO)(PHPh$_2$)),[12] a set of complexes which strongly suggests that good π-acceptor ligands are required to stabilize the addition products. This is also consistent with the need to accommodate the extra electrons beyond the 48 normally required for a stable triangular cluster. That π-acceptor character is not the only requirement is suggested by the instability, except under CO atmosphere, of the hexa- and heptacarbonyl derivatives relative to the apparent stability of the isocyanide complex, despite the fact that CO is a better π acceptor than isocyanide.

Comparison of the NMR parameters (Table I and structure V) for the 46-electron clusters, I and II, with those for the 50-electron species, III and IV, shows several interesting features. As expected,[10] the longer M–M distances in III and IV are reflected in strongly increased shielding for the bridging phosphorus atoms, the changes ranging from −80 to −240 ppm. The unique phosphorus bridges, P(2), in I and II are less deshielded than the other bridges and experience a smaller shift on going to III and IV. Presumably, this is because of the change in orientation of the unique bridge relative to the M_3 ring. In I and II, the bridge involving P(2) is nearly perpendicular to the M_3 plane and apparently experiences much less deshielding in this position than do the other phosphorus bridges, which are approximately in the M_3 plane. In all cases the bridges on iridium are more shielded than those on rhodium.

The change in orientation of the unique phosphorus bridge is also evident in the two-bond P–P couplings, J(1,2), involving this bridge. They change from 24 and 25 Hz in I and II to 144 and 160 Hz in III and IV, as expected for pseudocis and pseudotrans interactions. The associated change in the long-range Rh–P couplings is more puzzling. These are generally small (<5 Hz) except that, in IV, the values involving the basal rhodium atoms are much larger, 50–70 Hz for J(1,5′). The reason for this change is not evident, since any possible explanations involving electron counts or transmission pathways through the rhodium centers would apply to at least some of the other bridges in I–IV.

The weaker bonding and enhanced electron count in IV also result in a general reduction in the magnitude of Rh–P coupling relative to that in II. This is especially marked for coupling between the apical rhodium and its attached phosphorus bridges, J(1,4). This coupling decreases from 128 Hz in II to 35 Hz in IV and correlates with the increased M–P bond lengths (2.27 to 2.37 Å) in the iridium analogues.

Experimental Section

(a) Synthesis and Spectroscopic Studies. Data relating to the characterization of the complexes are given in the tables, under Results, and in the preparative descriptions below. Microanalysis was by the Canadian Microanalytical Service, Vancouver, BC, Canada. Infrared spectra were recorded in KBr disks from 4000 to 400 cm^{-1} with an accuracy ±3 cm^{-1} on a Perkin-Elmer 283 grating spectrophotometer calibrated against polystyrene film.

^{1}H and ^{31}P NMR spectra were recorded at 250.1 and 101.3 MHz, respectively, on a Bruker WM250 Fourier transform spectrometer. The solvent was CH_2Cl_2, and a lock signal was derived from the deuterium resonance of a capillary insert containing C_6D_6. For ^{31}P spectra, protons were decoupled by broad-band ("noise") irradiation, and chemical shifts were measured relative to external $P(OMe)_3$ and are reported in parts per million relative to 85% H_3PO_4 by using a conversion factor of +141 ppm. Positive chemical shifts are downfield of the reference. Simulated NMR spectra were calculated on an IBM 3090 computer and plotted on a Tektronix 4010 graphics screen for preliminary work or a Calcomp 1039 plotter for final data. The programs used were a locally constructed package based on UEAITR[27] and NMRPLOT.[28]

Except as noted below, all operations were carried out under an atmosphere of dry nitrogen and with standard Schlenk tube techniques. Solvents were dried by appropriate methods and distilled under nitrogen prior to use. $[Ir_2Cl_2(coe)_4]$ (coe = cyclooctene) was synthesized as

(27) Johannsen, R. B.; Ferreti, J. A.; Harris, R. K. *J. Magn. Reson.* **1970**, *3*, 84–93.
(28) Swalen, J. D. In *Computer Programs for Chemistry*; Detar, D. F., Ed.; W. A. Benjamin: New York, 1968; Vol. I.

previously described,[11] except that ammonium hexachloroiridate(IV) was used instead of hexachloroiridate(III). The cluster $[Rh_3(PPh_2)_3(CO)_3(PPh_3)_2]$ was synthesized according to the method of Billig et al.[13] Diphenylphosphine was obtained commercially (Aldrich Chemical Co.) and was used without further purification.

$[Ir_3(\mu\text{-}PPh_2)_3(CO)_3(PPh_2CH_2PPh_2)]$ (I). Carbon monoxide was bubbled vigorously through a solution of $[Ir_2(coe)_4Cl_2]$ (0.30 g, 0.33 mmol) in benzene (20 mL), resulting in rapid precipitation of a dark green solid, which is probably the polymer $[IrCl(CO)_3]_n$. Diethylamine (0.065 mL, 0.65 mmol) was added dropwise to the stirred mixture, and after 10 min a very pale yellow solution had formed. Addition of diphenylphosphine (0.11 mL, 0.65 mmol) caused an immediate change to a red-brown solution containing a mixture of $[Ir_3(PPh_2)_3(CO)_5]$ and $[Ir_3(PPh_2)_3(CO)_6]$. After being stirred for a further 30 min, the solution was filtered and the solvent removed in vacuo. The sticky red residue was dissolved in dichloromethane (15 mL), dppm (0.085 g, 0.22 mmol) was added, and stirring was continued for 2 h. Solvent was reduced in vacuo to about 5 mL, the solution transferred to an alumina column, and a pink-red band eluted with benzene. Removal of the solvent in vacuo, followed by crystallization of the residue from dichloromethane and hexanes gave the product as dark red cubes (0.070 g, 0.044 mmol). IR (cm^{-1}): ν(CO) = 1945 m, br, 1914 s, br. Anal. Calcd for $C_{64}H_{51}O_3P_5Ir_3$: C, 48.0; H, 3.21. Found: C, 47.1; H, 3.38.

$[Rh_3(\mu\text{-}PPh_2)_3(CO)_3(PPh_2CH_2PPh_2)]$ (II). Dppm (0.026 g, 0.068 mmol) was added to a stirred solution of $[Rh_3(PPh_2)_3(CO)_3(PPh_3)_2]$ (0.10 g, 0.068 mmol) in dichloromethane (15 mL). The color changed rapidly from dark green to bright emerald green. After 10 min, solvent was removed in vacuo and the residue crystallized from dichloromethane and hexanes to yield the product as green-black crystals (0.070 g, 0.053 mmol). IR (cm^{-1}): ν(CO) = 1932 s, 1925 sh. Anal. Calcd for $C_{64}H_{51}O_3P_5Rh_3$: C, 57.7; H, 3.86. Found: C, 57.3; H, 3.84.

$[Ir_3(\mu\text{-}PPh_2)_3(CO)_3(PPh_3)_2]$. A mixture of $[Ir_3(\mu\text{-}PPh_2)_3(CO)_5]$ and $[Ir_3(\mu\text{-}PPh_2)_3(CO)_6]$ (0.30 g, 0.23 mmol) in dichloromethane (10 mL) was prepared from $[Ir_2(coe)_4Cl_2]$ as described above. Triphenylphosphine (0.12 g, 0.46 mmol) was added to the stirred solution, and the color changed from red to green-black. After 30 min, solvent was removed in vacuo, the residue dissolved in a minimum of benzene, and the solution transferred to an alumina column. A green-black band was eluted with benzene, solvent was removed in vacuo, and crystallization of the residue from dichloromethane and hexanes gave the product as black crystals (0.045 g, 0.026 mmol). IR (cm^{-1}): ν(CO) = 1970 s, 1920 s, 1910 sh. Anal. Calcd for $C_{75}H_{60}Ir_3O_3P_5$: C, 51.7; H, 3.47. Found: C, 51.1; H, 3.56.

$[Ir_3(\mu\text{-}PPh_2)_3(CO)_5(t\text{-}BuNC)_2]$ (III). A solution of *tert*-butyl isocyanide (0.006 s, 0.072 mmol) in dichloromethane (1 mL) was added dropwise to a stirred dichloromethane solution (10 mL) of $[Ir_3(\mu\text{-}PPh_2)_3(CO)_3(PPh_3)_2]$ (0.050 g, 0.029 mmol) that had been previously saturated with carbon monoxide. The color changed from deep red to orange-yellow. After 10 min, solvent was removed in vacuo and the residue crystallized from dichloromethane and hexanes to give the product as bright yellow crystals (0.030 g, 0.021 mmol). IR (cm^{-1}): ν(CO) = 2165 m, 2130 m, 1940 m, 1925 m, 1885 s. Anal. Calcd for $C_{49}H_{48}Ir_3N_2O_3P_3$: C, 42.6; H, 3.50; N, 2.03. Found: C, 41.2; H, 3.74; N, 2.94.

A similar procedure using a mixture of $[Ir_3(\mu\text{-}PPh_2)_3(CO)_5]$ and $[Ir_3(\mu\text{-}PPh_2)_3(CO)_6]$, prepared as above, instead of $[Ir_3(\mu\text{-}PPh_2)_3(CO)_3(PPh_3)_2]$ gave the same product but a much lower yield.

$[Rh_3(\mu\text{-}PPh_2)_3(CO)_5(t\text{-}BuNC)_2]$ (IV). A solution of *tert*-butyl isocyanide (0.008 g, 0.096 mmol) in dichloromethane (1 mL) was added dropwise to a stirred solution of $[Rh_3(PPh_2)_3(CO)_3(PPh_3)_2]$ (0.050 g, 0.038 mmol) in dichloromethane (5 mL). The color changed rapidly from olive green to yellow-orange. After 10 min, solvent was removed in vacuo and the oily residue recrystallized from dichloromethane and hexanes to give the product as pale yellow crystals (0.025 g, 0.023 mmol). IR (cm^{-1}): ν(CO) = 2150 m, 2120 m, 1957 m, 1940 m, 1905 s. This product decomposed in storage and transit, and we were unable to obtain analytical data. The infrared spectrum was identical with that of the corresponding iridium complex, whose structure was confirmed by X-ray diffraction, and the analysis of the ^{31}P NMR data is given under Results.

(b) X-ray Data Collection. Compounds I ($[Ir_3(\mu\text{-}PPh_2)_3(CO)_3(dppm)]$), II ($[Rh_3(\mu\text{-}PPh_2)_3(CO)_3(dppm)]$), and III ($[Ir_3(\mu\text{-}PPh_2)_3(CO)_5(t\text{-}BuNC)_2]$) were prepared as described above, and crystals suitable for study by X-ray diffraction were grown by recrystallization from dichloromethane/hexanes. Preliminary photographic work was carried out with Weissenberg and precession cameras using Cu Kα radiation. After establishment of symmetry and approximate unit cells, the crystals were transferred to one of two diffractometers (see Table II) and the unit cells refined by least-squares methods employing pairs of centering measurements. There was no evidence of decomposition for any of the crystals during data collection.

Measurements on the CAD4 diffractometer used the NRCCAD modification of the Enraf-Nonius program[29] and the "Profile" $\omega/2\theta$ scan developed by Grant and Gabe.[30] Three standard reflections were measured every hour to check crystal stability, and three others were measured ever 400 reflections to check crystal orientation. Lorentz and polarization factors were applied, and the data were corrected for absorption by using an empirical method based on the work of North et al.[31] as implemented in the CAD4 structure determination package.

The Picker four-circle instrument was automated with a PDP11/10 computer and used a $\theta/2\theta$ step scan with 160 steps of 0.01° in 2θ, counting for 0.25 s per step. Background measurements were for 20 s at each end of the scan. Each batch of 50 reflections was preceded by the measurement of three standard reflections, and after application of Lorentz and polarization factors, each batch was scaled to maintain the sum of the standards constant. Absorption corrections were applied by a numerical integration using a Gaussian grid and with the crystal shape defined by perpendicular distances to crystal faces from a central origin.

(c) Structure Solution and Refinement. The structures were found and refined by using the SHELX-76 program package,[32] and illustrations were drawn by using ORTEP.[33] The atomic scattering factors used were for neutral atoms, with corrections for anomalous dispersion.[34] The structures were solved by direct methods, developed by standard Fourier synthesis procedures using difference maps, and refined by the method of least squares minimizing $\sum w\Delta^2$ where $\Delta = ||F_o| - |F_c||$. The weights were obtained from counting statistics by using $w = 1/(\sigma^2(F) + 0.001F^2)$. For I and II, all iridium, rhodium, and phosphorus atoms were treated anisotropically, and the phenyl rings were refined as rigid groups, except for those attached to P(2). These latter phenyl groups lie on or across the molecular symmetry planes of I and II defined by O(1), C(1), M(1), P(2), C(37) and the midpoint of M(2)–M(2'). For III, all atoms were treated anisotropically except for those of the phenyl rings, which were treated isotropically. Hydrogen atoms were not located in any of the three structures. The final difference maps gave no indication that any material had been overlooked.

Acknowledgment. We thank the Natural Sciences and Engineering Research Council of Canada and the University of Victoria for research grants, Mrs. K. Beveridge for technical assistance in the crystal structure determinations, and Mrs. C. Greenwood for recording the NMR spectra.

Supplementary Material Available: For compounds I–III, unit cell, data collection, and refinement parameters (Table S1), fractional atomic coordinates and isotropic temperature parameters for all atoms (Tables S2–S4), anisotropic temperature factors for the heavy atoms (Tables S5–S7), interatomic distances (Tables S8–S10), bond angles (Tables S11–S13), and selected intermolecular distances (Tables S14–S16) (20 pages); observed and calculated structure factor amplitudes (Tables S17–S19) (33 pages). Ordering information is given on any current masthead page.

(29) Le Page, Y.; Gabe, E. J.; White, P. S. NRCCAD modification of the Enraf-Nonius program, Chemistry Division, National Research Council of Canada, Ottawa, Canada.
(30) Grant, D. F.; Gabe, E. J. *J. Appl. Crystallogr.* **1978**, *11*, 114–120.
(31) North, A. C. T.; Phillips, D. C.; Mathews, F. S. *Acta Crystallogr.* **1968**, *A24*, 351–359.
(32) Sheldrick, G. M. SHELX-76. A Computer Program for Crystal Structure Determination. University of Cambridge, Cambridge, England, 1976.
(33) Johnson, C. K. ORTEP: A Fortran thermal ellipsoid plot program for crystal structure illustrations. Report ORNL-3794; Oak Ridge National Laboratory: Oak Ridge, TN, 1965.
(34) Cromer, D. T.; Waber, J. T. In *International Tables for X-Ray Crystallography*; Ibers, J. A., Hamilton, W. C., Eds.; Kynoch Press: Birmingham, England, 1974; Vol. IV.